Influence of Atomic Vacancies on the Properties of Transition-Metal Oxides. I. TiO_x and VO_x †

John B. Goodenough
Lincoln Laboratory, Massachusetts Institute of Technology, Lexington, Massachusetts 02173
(Received 23 July 1971)

After a brief review of the principal features associated with energy-band diagrams of ideal transition-metal monoxides having localized vs itinerant *d* electrons, modification of these diagrams is discussed for real crystals in the systems TiO_x and VO_x, which have itinerant *d* electrons. Each of these systems contains approximately 16% spontaneous atomic vacancies, and physical arguments are presented for the influence of these vacancies on the one-electron energies for both ordered and disordered crystals. It is argued that isolated cation vacancies tend to trap two holes, and anion vacancies to trap two electrons. The character of these trap states can be described for ordered systems. Disordered vacancies appear to create energy bands having features similar to those found in amorphous materials. The rather striking physical properties of the VO_x system can be qualitatively understood from physical arguments alone, as can the contrast between these properties and those found in TiO_x.

I. INTRODUCTION

Monoxides of the first-row transition elements, excluding CuO, provide an isostructural series of compounds in which some members have itinerant *d* electrons while others contain localized *d* electrons. In addition, their rocksalt structure is simple and therefore attractive for theoretical analysis. Although magnetic and crystallographic data have been available for some time, a chemical characterization adequate for interpretation of transport and optical properties has only recently been undertaken. Because experimental information about the character of the transition from localized to itinerant behavior of the outer *d* electrons is so fundamental for solid-state theory, it is important to develop the correct conceptual framework within which to interpret experimental data. This paper attempts to introduce the concepts essential to the construction of such a framework and to show how they may be applied to obtain semiempirical energy-level diagrams for the separate compounds. Previous workers have attempted band calculations for ideally stoichiometric compounds, [1] and these energy diagrams indicate how the one-electron energies vary with wave vector within any energy band. However, there is still a need to establish more gross features of the energy diagrams, and it is to this task that this paper is addressed. In particular, the influence of atomic vacancies is considered. After a general introduction to the energy diagrams for ideal crystals, this paper contains a discussion of the systems TiO_x and VO_x, which have itinerant *d* electrons. Native defects in monoxides having localized *d* electrons require similar attention for any adequate interpretation of the transport and optical data.

II. IDEAL CRYSTALS

Although native defects play a critical role in determining the physical properties of solids, nevertheless they represent perturbations of the ideal stoichiometric structure. Therefore any discussion must begin with the ideal crystal.

If E_I is the energy required to take an electron from an M^+ cation and to place it on an O^- anion and if E_M is the electrostatic Madelung energy for an $M^{2+}O^{2-}$ crystal, then the pertinent one-electron energies at the ions would be as shown schematically in the left-hand and right-hand columns of Fig. 1. Since electron transfer in a crystal is never complete, the energy $(E_M - E_I)$ of Fig. 1 is generally taken for the effective charges on the ions. This is the starting point of any energy-band calcula-

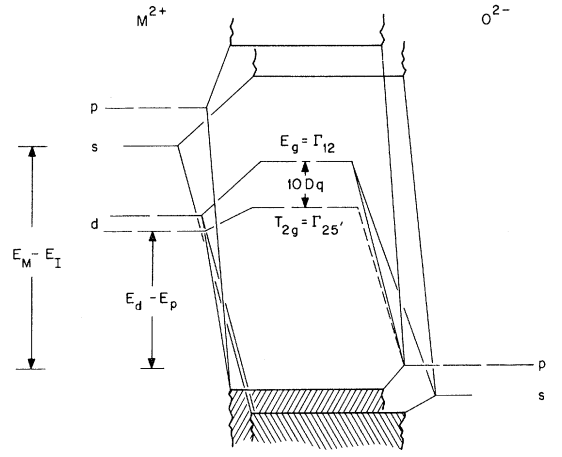

FIG. 1. Schematic one-electron energies for transition-metal monoxides having the rocksalt structure and localized 3*d* electrons.

tion.

The outer s and p electrons, which are primarily responsible for the binding energy of the crystal, interact strongly with the near-neighbor atoms. Therefore these electrons are always itinerant and may be described by conventional band theory. Like zinc blende, the rocksalt structure is composed of two interpenetrating, fcc arrays: a cation and an anion array. Because each array has the same symmetry, the symmetrized orbitals belong to similar irreducible representations, and there is covalent mixing between the s and p orbitals of the two types of ions. Covalent mixing also splits the bands of one-electron energies: The more stable, bonding bands are occupied and primarily anionic in character, the less stable, antibonding bands are empty and primarily cationic in character. The top of the occupied bands belongs to an O^{2-} $2p$ band and occurs at the center of the Brillouin zone. The bottom of the empty bands belongs to an $M^{2+}s$ band and is also at the center of the Brillouin zone. The magnitude of the energy gap E_g increases with $E_M - E_I$. Theoretical estimates and a shoulder in the optical-absorption spectrum of NiO are consistent with an $E_g \approx 5.5$ eV in this compound. Transition elements to the left of nickel in the Periodic Table are more ionic, so that an

$$E_g \gtrsim 5.5 \text{ eV} \tag{1}$$

should hold for all monoxides of the first-row transition elements (excluding CuO).

Stable oxides have their Fermi energy within this large energy gap E_g, and it is possible to determine the number of outer d electrons per transition-metal ion from the formal valence states of the ions. This is the significance of a formal-valence-state nomenclature for these ions.

Description of the outer d electrons begins with one-electron wave functions of the crystal-field, localized orbitals in which covalent mixing with the s and p orbitals at nearest-neighbor anions and cations is included. Since covalent mixing only occurs between symmetrized orbitals having the same irreducible representations, covalent mixing does not change the symmetry properties of these orbitals, which may be determined from the angle-dependent part of the ionic d functions:

$$\begin{aligned} f_0 &\sim [(z^2 - x^2) + (z^2 - y^2)]/r^2 = 3\cos^2\theta - 1, \\ f_{\pm 1} &\sim 2(zx \pm iyz)/r^2 = \sin 2\theta\, e^{\pm i\phi}, \\ f_{\pm 2} &\sim [(x^2 - y^2) \pm i2xy]/r^2 = \sin^2\theta\, e^{\pm i2\phi}. \end{aligned} \tag{2}$$

The cubic crystalline fields split these fivefold-degenerate atomic functions into threefold-degenerate f_t orbitals of T_{2g} symmetry:

$$f_{xy} \sim xy/r^2, \quad f_{yz} \sim yz/r^2, \quad f_{zx} \sim zx/r^2, \tag{3}$$

and twofold-degenerate f_e orbitals of E_g symmetry:

$$f_{z^2} \sim [(z^2 - x^2) + (z^2 - y^2)]/r^2, \quad f_{x^2-y^2} \sim (x^2 - y^2)/r^2. \tag{4}$$

In the rocksalt structure, the f_e orbitals σ bond with the anion s_σ and p_σ orbitals, the f_t orbitals π bond with the anion p_π orbitals and σ bond with nearest-neighbor cation s_c and p_c orbitals. Since σ bonding is stronger than π bonding and covalent mixing with anion s and p orbitals destabilizes less stable d wave functions while stabilizing the anion s and p functions, the orbitals of E_g symmetry are made less stable than those of T_{2g} symmetry, and the crystalline d orbitals are

$$\psi_e = N_\sigma(f_e - \lambda_s\phi_s - \lambda_\sigma\phi_\sigma), \tag{5}$$

$$\psi_t = N_\pi(f_t - \lambda_\pi\phi_\pi + \lambda_c\phi_c), \tag{6}$$

where N_σ and N_π are normalization constants. The ϕ_i are properly symmetrized s and p wave functions at the nearest-neighbor anions and cations, and the covalent mixing parameters for a d^n manifold are

$$\lambda_i \sim (f, \mathcal{H}'\phi_i)/\Delta_i, \tag{7}$$

where Δ_i is the energy difference between f and ϕ_i for a d^{n+1} configuration. The energy operator $\mathcal{H}'$ represents the perturbation of the electron potential for ϕ_i as a result of the presence of the cation with ionic orbital f.

The crystal-field orbitals of Eqs. (5) and (6) provide a one-electron description of the d orbitals. The one-electron energies are shown in Fig. 1. However, where the d electrons are localized, as at an isolated transition-metal ion substituted into an MgO host, intra-atomic correlations and spin-orbit coupling must also be introduced. The result is a multielectron description for the d-state manifold, and the various multielectron states $^{(2S+1)}\Gamma$ have discrete energies relative to one another and to the broad-band edges that may be determined from optical and EPR measurements. Here S is the net atomic spin, and Γ is the symmetry notation: A_{1g}, A_{2g}, E_g, T_{1g}, T_{2g} replacing the $L = S$, P, D, F, $\cdots$ angular-momentum designations appropriate for spherical symmetry. In a salt like MnO, on the other hand, interactions between the d-state manifolds on neighboring atoms must also be introduced. In the localized-electron limit, the dominant contribution to this interaction is superexchange, the mixing into the isolated-ion ground state of electron-transfer excited states. Two types of electron transfer states are considered: transfer from a d orbital on one cation to a d orbital on another (delocalization superexchange) and two-electron transfer from an anion to two neighboring cations (correlation superexchange). These interactions give rise to long-range magnetic order and exchange striction below a magnetic-ordering temperature, and at lower temperatures the one-ion

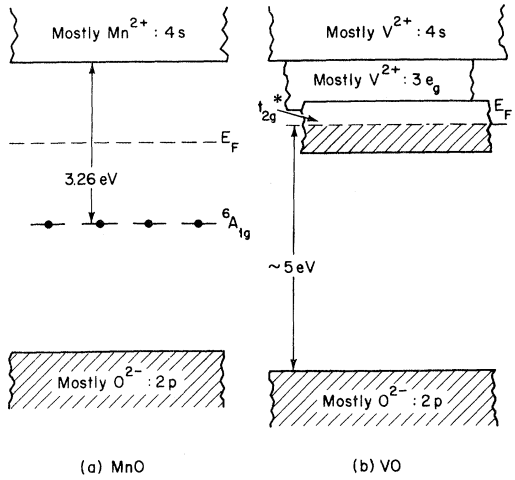

FIG. 2. Energy diagrams for stoichiometric ideally dense transition-metal monoxides: (a) MnO and (b) VO.

levels are broadened into a narrow, one-magnon band of spin-wave energies. The resulting energy diagram for antiferromagnetic MnO is shown in Fig. 2(a). Not shown are the excited d^5 configurations or the d^6 configuration, which has an energy above the bottom of the Mn^{2+}: 4s band.

Where the d electrons are itinerant, on the other hand, the crystal-field orbitals of Eqs. (5) and (6) provide the localized basis functions from which to build a tight-binding theory. With these basis functions, only the fcc cation subarray need be considered. Both nearest-neighbor and next-nearest-neighbor interactions are important. The next-nearest-neighbor interactions involve two transfer energies:

$$b_\sigma = (\psi_{ei}, \mathcal{H}'\psi_{ej}) \sim \epsilon_\sigma(\psi_{ei}, \psi_{ej}) \sim \epsilon_\sigma N_\sigma^2(\lambda_\sigma^2+\lambda_s^2), \quad (8)$$

$$b_\pi = (\psi_{ti}, \mathcal{H}'\psi_{tj}) \sim \epsilon_\pi(\psi_{ti}, \psi_{ti}) \sim \epsilon_\pi N_\pi^2(\lambda_\pi^2+\lambda_c^2), \quad (9)$$

where ϵ_σ and ϵ_π are one-electron energies. Similarly the nearest-neighbor interactions contain two transfer energies:

$$b_{\sigma\pi} = (\psi_{ei}, \mathcal{H}'\psi_{tj}) \sim \epsilon_{\sigma\pi}(\psi_{ei}, \psi_{tj}) \sim \epsilon_{\sigma\pi} N_\sigma N_\pi \lambda_\pi \lambda_\sigma, \quad (10)$$

$$b_{cc} = (\psi_{ti}, \mathcal{H}'\psi_{tj}) \sim \epsilon_c(\psi_{ti}, \psi_{tj}), \quad (11)$$

where the overlap integral (ψ_{ti}, ψ_{tj}) increases sensitively with decreasing cation separation R. In tight-binding theory, polar terms are considered to have the same energy as nonpolar terms, an approximation neglecting electron correlations that are important where the bands are narrow. In this limit, the energy bands are calculated in first-order perturbation theory, and the bandwidth is proportional to a transfer energy b_λ.

Among the monoxides of the first transition series, only TiO_x and VO_x have itinerant d electrons. From the formal valence states Ti^{2+} and V^{2+}, the number of d electrons per cation in these compounds is ≈ 2 and ≈ 3, respectively, and the orbitals ψ_e are empty. Since all the oxygen p orbitals σ bond with the empty f_e orbitals, π bonding with the partially filled f_t orbitals should be relatively small. Therefore we may anticipate a $\lambda_\sigma \gg \lambda_\pi$. Furthermore, the orbitals ψ_e and ψ_t are split by 10 $Dq > 1$ eV, so that for $b_{\sigma\pi} < 10\,Dq$ the cross terms involving $b_{\sigma\pi}$ require second-order perturbation theory. Covalent mixing between nearest-neighbor cations via those cross terms increases the radial extension of ψ_t, and b_{cc} becomes changed to a lumped nearest-neighbor transfer energy

$$b_{\rm nn} \sim \epsilon[(\psi_{ti}, \psi_{tj}) + 2\lambda N_\sigma N_\pi \lambda_\sigma \lambda_\pi], \quad (12)$$

where $\lambda \sim b_{\sigma\pi}/(10\,Dq)$. Similarly a lumped next-nearest-neighbor transfer energy would be

$$b_{\rm nnn} \sim \epsilon_\sigma[N_\sigma^2(\lambda_\sigma^2+\lambda_s^2) - 2\lambda N_\sigma N_\pi \lambda_\sigma \lambda_\pi]. \quad (13)$$

In this approximation, the one-electron ψ_e orbitals of Fig. 1 are transformed into a narrow σ^* band of itinerant-electron orbitals having a bandwidth

$$W_\sigma \sim 12\, b_{\rm nnn} \sim \epsilon_\sigma \lambda_\sigma^2, \quad (14)$$

and the ψ_t orbitals are transformed into a narrow, cation-sublattice t_2^* band of width

$$W_t \sim 24\, b_{\rm nn}(R). \quad (15)$$

The factors 12 and 24 in Eqs. (14) and (15) represent twice the numbers $z_{\rm nnn}$ and $z_{\rm nn}$ of next-nearest and nearest neighbors, respectively.

A schematic band structure for ideally dense and stoichiometric VO is shown in Fig. 2(b). The three outer 3d electrons per V^{2+} ion just half-fill the t_2^* band. Vanadium is far enough to the left in the first-row transition series that localized 3d orbitals of a V^{2+} ion would have energies close to the edge of the 4s band, and considerable overlap of the 4s and 3d bands can be anticipated. However, the orbitals in the bottom half of the t_2^* bands, though antibonding with respect to the anion array, are bonding with respect to the cation array. Therefore, the Fermi energy E_F should lie below the σ^* bands, probably about 2 eV below the bottom of the 4s band. In TiO, the Fermi energy would be even less stable relative to the edge of the 4s band, probably approaching within 1 eV of it.

At a free ion, successive ionization energies show that an electrostatic energy $U \approx 15$ eV is required to make a 3d-electron transfer

$$2M^{2+} \rightarrow M^{3+} + M^{+}. \quad (16)$$

This energy is somewhat smaller for the lighter ions Ti^{2+} and V^{2+} because of 4s-4p hybridization. In the free-ion limit successive valence states for the ion are separated by this energy, as illustrated in Fig. 3 for an ideal VO with large lattice parameter. On the other hand, in the limit where tight-

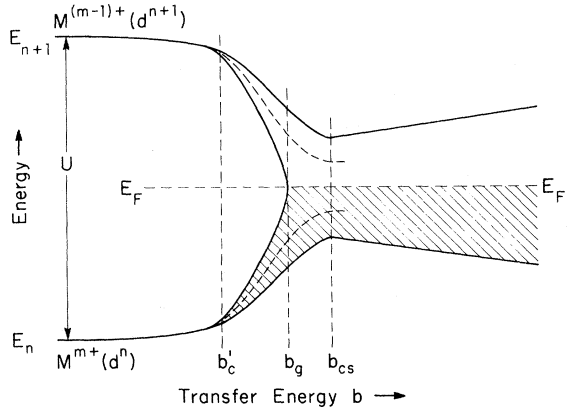

FIG. 3. Pseudoparticle energy diagram as a function of the nearest-neighbor, spin-independent transfer energy b for a half-filled band, or half-filled degenerate bands.

binding theory is applicable this energy must be reduced to $U < W_t$, since a $U = 0$ is assumed in the theory. As Mott[2] has pointed out, the energy U is reduced in a solid because electron transfers from neighboring ions partially screen the outer electrons from their parent nuclei, giving them a larger radial extension. The less tightly bound the electrons to a particular nucleus, the smaller are the successive ionization potentials; and where an electron becomes delocalized so as to belong collectively to all the like atoms of a periodic array, there the energy U is screened sufficiently that $U < W$. In the case of VO,

$$U = [\psi_t(\vec{r} - \vec{R}_i)\,\psi_t(\vec{r}' - \vec{R}_i)\,,\ V_i\psi_t(\vec{r} - \vec{R}_i)\psi_t(\vec{r}' - \vec{R}_i)]\,, \tag{17}$$

$$V_i = (e^2/|\vec{r} - \vec{r}'|)\,e^{-\xi|\vec{r}-\vec{r}'|}\,,$$

where the screening parameter $\xi = \xi(b_{nn}/U)$ increases monotonically with increasing transfer energy b_{nn} and $\xi(0) = 0$, where $b_{nn} = 0$ at $R = \infty$ increases with decreasing R. This reasoning leads to a pseudoparticle energy diagram as a function of b_{nn} like that of Fig. 3. Where $b_{nn} \ll U$, the electron-transfer excited states, which give delocalization superexchange, are treated in second-order perturbation theory. Therefore the change in energy is

$$\mathcal{H}_{ij}^{S} = -2t_{ij}^2/U\,, \tag{18}$$

where t_{ij} is the spin-dependent transfer energy, localized f_t orbitals giving each V^{2+} ion a $^4A_{2g}$ ground state. The extra factor 2 comes from the fact that there is transfer from $\vec{R}_j$ to $\vec{R}_i$ as well as from $\vec{R}_i$ to $\vec{R}_j$. The rotational transformation between spins α, β, and α', β' is

$$\alpha = \cos(\tfrac{1}{2}\theta)\alpha' + \sin(\tfrac{1}{2}\theta)\beta'\,,$$
$$\beta = -\sin(\tfrac{1}{2}\theta)\alpha' + \cos(\tfrac{1}{2}\theta)\beta'\,. \tag{19}$$

Since spin is conserved in an electron transfer, the Pauli exclusion principle requires that an electron transferred from a half-filled ψ_{ti} orbital to a half-filled ψ_{tj} orbital be antiparallel to the spin of ψ_{tj}, and hence the net spin $\vec{S}_j$ at $\vec{R}_j$. This makes $t_{ij} = b_{ij}\sin(\frac{1}{2}\theta_{ij})$, and Eq. (18) becomes

$$\Delta\mathcal{H}_{ij}^{S} = +2(2b_{ij}^2/4S^2U)\vec{S}_i \cdot \vec{S}_j\,, \tag{20}$$

which has the Heisenberg form for an antiferromagnetic interaction energy between spins at two neighboring atoms. However, as b_{ij} increases, U decreases and the ratio b^2/U necessarily increases so long as the perturbation expansion is valid. At some critical value b_c, where $b_c/U < 1$, this expansion must break down. This critical value would be marked by a maximum in the Néel temperature,[3] as is illustrated schematically in Fig. 4. In the narrow interval $b_c < b_{nn} < b_g$ of Fig. 3, where $W_{nn} \approx U$, the energy U must be introduced explicitly into an itinerant-electron formalism. Hubbard[4] has discussed this problem in a series of papers. Splitting of the half-filled band by electron correlations at transfer energies $b_{nn} < b_g$ will be referred to as electron-correlation splitting. Hubbard[4] was the first to show that within the itinerant-electron formalism the two pseudoparticle bands have a width $W_b \approx 2zb$ even in the limit $U \gg W_b$. Explicit in Fig. 3, on the other hand, is the assumption that for $b < b_c$ there is a phase transition into a localized-electron state in which the bandwidths of successive d-state manifolds are essentially the widths of the spin-wave spectrum. Such an assumption is compatible with exciton absorption spectra in antiferromagnetic salts like Cr_2O_3, but it is at variance with the usual assumptions implicit in band theory.

In the localized-electron domain $b_{nn} \leq b_c$, the

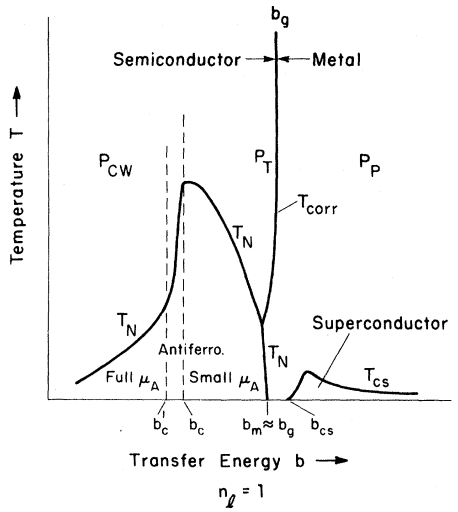

FIG. 4. Schematic b-T phase diagram for a half-filled band, or half-filled degenerate bands. P_{CW}, P_T, and P_P refer, respectively, to Curie-Weiss, transitional, and Pauli paramagnetism; μ_A is the atomic moment measured by neutron diffraction.

paramagnetic susceptibility above T_N would be described by a Curie-Weiss law, and the molar Curie constant would be calculable from crystal-field theory as

$$C_m = Ng^2 S(S+1)\,\mu_B^2/3k\,, \tag{21}$$

where $S=\frac{3}{2}$ and $g=2$. Furthermore, the Weiss constant θ would be related to the Néel temperature T_N by molecular-field theory, giving a $|\theta| \sim T_N$. In the broad-band limit, on the other hand, the half-filled band would give a weak, temperature-independent Pauli paramagnetism. As illustrated in Fig. 5, the magnetic susceptibility must change from one limit to the other in an intermediate range of b_{nn}. Just how this change occurs as a function of the interaction parameter b has not been systematically studied, either theoretically or experimentally, although Evenson, Schrieffer, and Wang[5] have made an important theoretical contribution to this problem. It appears that spontaneous antiferromagnetism occurs for $b < b_m \approx b_g$ and that in some materials a nonvanishing U may cause an exchange-enhanced, temperature-dependent susceptibility in an interval $b_m < b < b_m + \Delta b$ even though no spontaneous magnetic order occurs,[6] whereas in others, such as metallic chromium where the Fermi surface "nests" in a Brillouin zone,[7] there may be a transition from antiferromagnetic order below T_N to Pauli paramagnetism above T_N. This suggests that a $b_m < b_g$ may occur in one compound and a $b_m > b_g$ in another. This issue is important for any interpretation of the real system VO_x. The temperature T_{corr} of Fig. 5 marks a possible phase change with increasing temperature from weakly correlated to strongly correlated itinerant electrons. This possibility arises because the higher entropy associated with randomly oriented, localized spins makes the line b_g slope as indicated in Fig. 4.

III. REAL TiO_x AND VO_x

A. General Considerations

A systematic investigation of several physical properties of the TiO_x and VO_x systems has now been carried out on the same samples of carefully characterized cast ingots.[8,9] Some of these properties are summarized in Fig. 6.

In addition to a lack of any spontaneous magnetic order and to low room-temperature resistivities, the monoxides of titanium and vanadium differ from the other monoxides of first-row transition elements in two other significant ways: (i) They each have a wide phase field, extending at high temperatures over the range of compositions $0.6 < x \leq 1.28$ in TiO_x and $0.75 \leq x \leq 1.33$ in VO_x, and (ii) they contain a large number of both cation and oxygen vacancies, about 16% of the lattice sites being vacant in stoichiometric TiO and VO. The vacancy concentration is relatively independent of preparation temperature, which means that the internal energy is reduced by the spontaneous creation of atomic vacancies.

A reduction of the internal energy by the spontaneous creation of atomic vacancies requires that there be a gain in cation-cation binding energy that is larger than any attendant loss in Madelung energy. According to Fig. 2(b), this requirement is satisfied in TiO_x and VO_x provided two conditions are met: (1) Introduction of atomic vacancies reduces the lattice parameter, thereby broadening the t_2^* bands so as to stabilize the occupied states in the bottom half of the bands, and (2) two electrons are trapped at each isolated anion vacancy, two holes are trapped at each isolated cation vacancy, thereby minimizing the attendant loss in Madelung energy.

Direct evidence for a reduction in lattice parameter with vacancy concentration has been obtained by pressure experiments.[10] Application of hydrostatic pressure at high temperatures, which tends to remove the vacancies, *increases* the cubic lattice parameter subsequently measured at atmospheric pressure. In disordered TiO, for example, this parameter increases from 4.17 to 4.26 Å.

There is no direct evidence for trapping of two electrons at each isolated anion vacancy, or two holes at each isolated cation vacancy. Therefore, I shall assume that this is the case and will argue that such an assumption leads to predictions that are consistent with observation.

How Fig. 2(b) must be modified to account for the trapping of bound charges at the atomic vacancies may be determined from physical arguments.

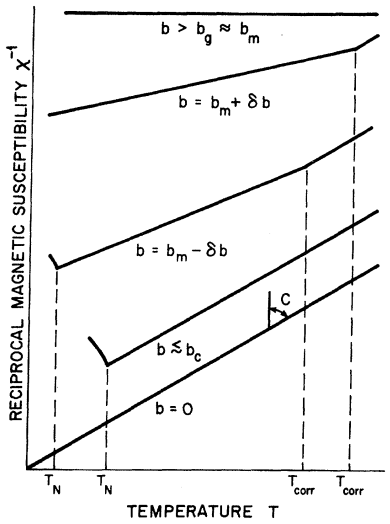

FIG. 5. Reciprocal magnetic susceptibility χ^{-1} vs temperature T for various values of the transfer energy b.

From Fig. 7, the t_{2g} orbitals at cations neighboring a cation vacancy not only fail to be stabilized by bonding with the cation t_{2g} orbitals normally at the vacancy, but also are more strongly destabilized by π-bond covalent mixing with the anions, since the anion p orbitals do not σ bond to the vacancy. Therefore, an isolated cation vacancy removes appropriately symmetrized orbitals from the bonding t_2^* bands and raises them above the Fermi energy E_F. So long as holes are localized at isolated cation vacancies, the energy of a second trapped hole lies below that of the first. The requirement of two trapped holes per isolated vacancy calls for two trap t_2^* V_C states above E_F per cation vacancy V_C. As the concentration of vacancies increases, these localized trap states may be transformed into "defect-band" states. However, since the d bands from which they are formed are themselves narrow, the defect-band states, which must be even more narrow, can be expected to be separated by an electrostatic energy U'. Therefore localized spins may be associated with partially filled defect bands.

Anion vacancies, on the other hand, not only stabilize the bonding t_2^*-band orbitals, but also strongly perturb the σ-bonding e_g and s orbitals on neighboring cations, as can also be seen from Fig. 7. These e_g and s orbitals are not destabilized by covalent mixing with the anion p_σ orbitals normally at the vacancy site; rather they are stabilized by the effective positive potential at the vacancy. In an analogy with color centers in the alkali halides, appropriately symmetrized e_g and s orbitals are lowered from the e_g and $4s$ σ^* bands above E_F to

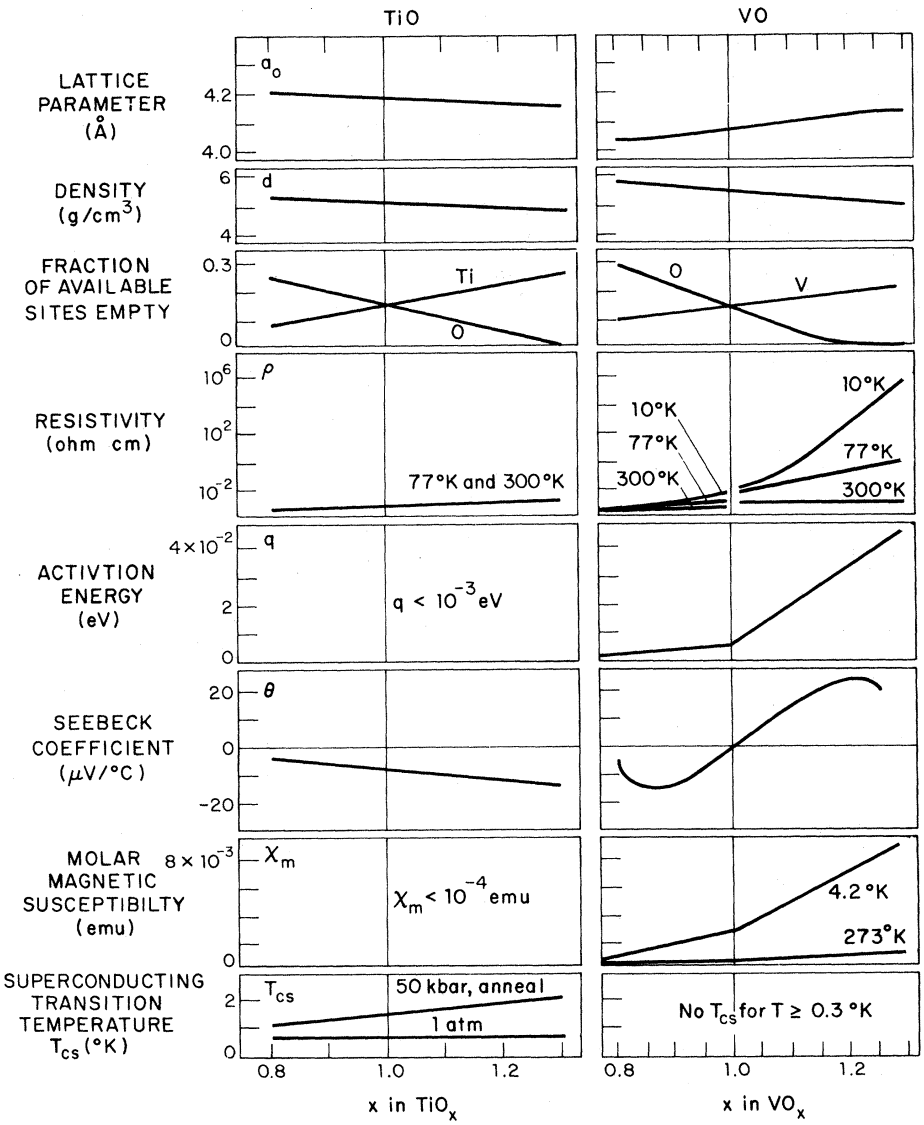

FIG. 6. Summary of the composition dependence of various physical properties in the systems TiO_x and VO_x, after Refs. 7 and 8.

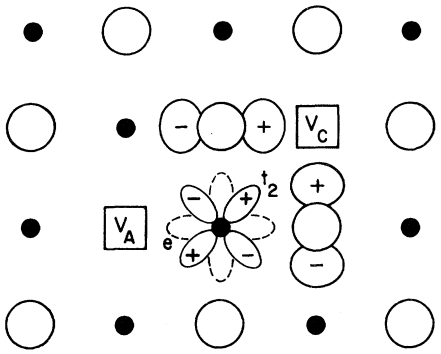

FIG. 7. Relative geometries of atomic orbitals and atomic vacancies in the systems TiO_x and VO_x.

trap-state levels below E_F. Where the concentration of anion vacancies is large, these trap orbitals become transformed into defect-band states. Because these trap states have a $4s$ as well as a $3d$ character, they may be broader than the defect-band states associated with trapped t_2^* holes at the cation vacancies. The requirement of two trapped electrons per anion vacancy would place two defect-band states per vacancy completely below E_F. However, the defect bands may be broad enough that this requirement is not strictly fulfilled. Broad defect bands would not be split in two by a $U' \neq 0$ and would not sustain localized spins.

B. TiO_x

Stoichiometric TiO has ordered vacancies if annealed at 900 °C. The ordered monoclinic structure, which is illustrated in Fig. 8, creates cation and anion vacancies within every third $(110)_c$ plane of the cubic (rocksalt) matrix.[11] Each vacancy has four unlike vacancies at next-nearest-neighbor unlike-atom positions. At each cation it is possible to identify a d_{xy}, d_{yz}, or d_{zx} orbital (x, y, and z axes referred to cubic axes) that are directed toward two nearest-neighbor cation vacancies. Appropriate symmetrization of these orbitals gives cation-vacancy trap orbitals that are destabilized relative to the other t_2^* orbitals. This destabilization occurs because the nearest-neighbor-anion p orbitals that would σ bond to the cation vacancies are available for strong π bonding, and covalent mixing destabilizes the antibonding d-like orbitals. The translational symmetry splits off two unstable d orbitals per cation vacancy, which represents the two trapped holes. Since there are two $3d$ electrons per formal-valence Ti^{2+} ion, the remaining orbitals from the t_2^* bands would be less than half-filled even in the absence of trap orbitals associated with the anion vacancies.

Two types of cations can be distinguished relative to the anion vacancies. Within the $(110)_c$ planes containing atomic vacancies, the cation $d_{3z^2-r^2}$ orbitals are directed toward two nearest-neighbor vacancies, one on each side of the cation, so that destabilization by σ bonding with nearest-neighbor anions is eliminated. This orbital, which is nonbonding with respect to the anion array, is stabilized by the positive potential created by the crystalline fields at the anion-vacancy sites. Therefore, these $d_{3z^2-r^2}$ orbitals can be expected to form a stable band below E_F. Actually the localized trap orbitals from which an anion-vacancy band would be constructed contain considerable $4s$ character due to $3d$-$4s$ hybridization. In addition, the remaining cations have either a $d_{3x^2-r^2}$ or a $d_{3y^2-r^2}$ orbital interacting with each anion vacancy, so that a localized trap orbital has the form

$$\phi^A_{\text{trap}} = a_1 d^{(1)}_{3z^2-r^2} + a_2(d^{(2)}_{3x^2-r^2} + d^{(3)}_{3y^2-r^2}) + a_3\phi_{4s}\,, \quad (22)$$

where the superscripts (1), (2), and (3) refer to the appropriate nearest-neighbor cations of an anion vacancy and ϕ_{4s} is a symmetrized $4s$ orbital from all the nearest-neighbor cations. In Eq. (22), the coefficient a_1 is the largest. The crystalline fields spread these electrons out into the anion-vacancy position, thereby literally trapping electrons at each anion vacancy in a manner similar to that observed in the anion-defect pyrochlore $PbRuO_3$.[12] By analogy with the color centers in alkali halides, it is reasonable to anticipate that the first electron per anion vacancy is reasonably well localized and that an electrostatic energy $U' \neq 0$ may be required to add a second electron. Therefore, the narrow anion-vacancy band in Fig. 9(a) is given two maxima in the density of states, but the entire defect band is assumed below E_F to give two electrons per anion vacancy.

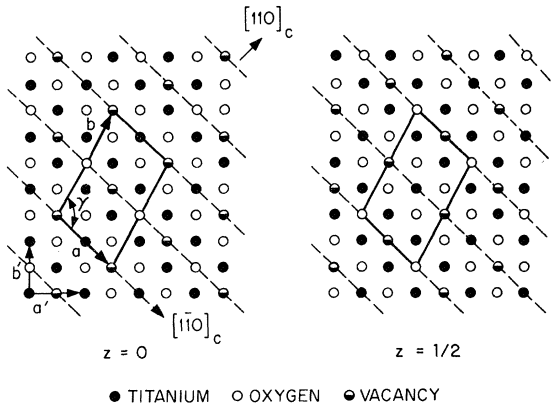

FIG. 8. $z = 0$ and $z = \frac{1}{2}$ planes of low-temperature, vacancy-order TiO. Solid lines designate monoclinic unit cell, dashed lines the $(110)_c$ planes of the high-temperature rocksalt structure. The $z = 0$ and $z = \frac{1}{2}$ planes are $(001)_c$ planes of the disordered rocksalt structure. After Ref. 11.

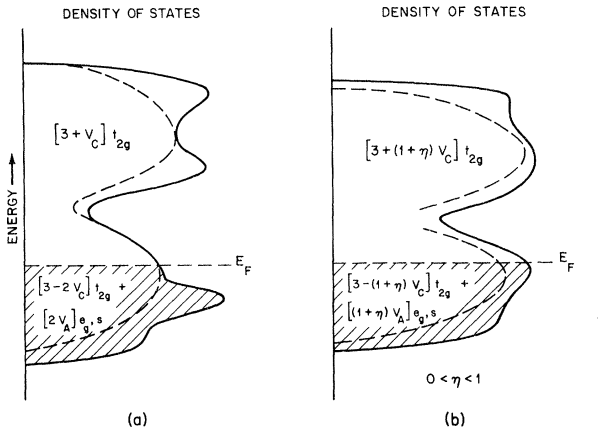

FIG. 9. Proposed density of states near the Fermi energy E_F for TiO: (a) ordered and (b) disordered atomic vacancies. At $x=1.0$, $V_C=V_A$.

The schematic diagram of Fig. 9(a) also illustrates the raising of $2[V_C]$ cation-vacancy trap orbitals from the lower-half of the t_2^* bands of Fig. 2(b) to the upper-half of these bands, where $[V_C]$ and $[V_A]$ represent the respective concentrations of cation and anion vacancies per cation or anion lattice site. The peak in the density of states at the energy of the second hole per cation vacancy is emphasized in the drawing in order to indicate that these trap orbitals may not be too unstable relative to the middle of the t_2^* bands. If $2[V_A]$ anion-vacancy trap orbitals lie below E_F, as shown, then the two $3d$ electrons per Ti^{2+} ion in TiO place the Fermi energy well below the middle of the t_2^* bands, as in "ideal" TiO represented by Fig. 2(b). It follows that TiO must be metallic so long as the Ti-Ti separation R is smaller than the critical separation R_c for $U \approx W_t$. I have given a semiempirical estimate of $R_c = 3.02$ Å for Ti^{2+} ions in oxides at room temperature and atmospheric pressure,[13] and an $R = 2.95$ Å is obtained from the room-temperature lattice parameter. Therefore, the entire analysis is consistent with the observation that TiO is a metal and becomes superconducting at lowest temperatures.

Disordered-vacancy TiO has been obtained by quenching from 1300 °C. The electrical conductivity and the superconducting transition temperature are dramatically reduced by vacancy disorder.[10] Where the vacancies are disordered, trapped holes and electrons are less easy to identify. Nevertheless it is reasonable to anticipate that isolated vacancies still trap two electrons or two holes. However, where a cation vacancy has an anion vacancy at a nearest-neighbor lattice site, there one cation-vacancy trap state may be annihilated by an anion-vacancy trap state. Thus the principal feature in a disordered case is a changing potential on going from cation to cation within the structure. Such a changing potential must reduce the electron mobility $\mu = e\tau/m^*$, not only by reducing the mean time τ for electron scattering, but also by narrowing the band to increase the effective mass m^*. In fact, there may also be some segregation of bonding states from antibonding states, which would tend to split the bands in two, because molecular orbitals associated with metal-metal pairs become a more natural basis than atomic orbitals for the formation of band states. Therefore Fig. 9(b) shows one trap state per vacancy in a band of localized or defect-band orbitals, a minimum in the center of the itinerant-electron t_2^* bands, and a broader band of second-hole or second-electron trap states numbering less than one per vacancy because of annihilation of cation and anion trap states at nearest-neighbor vacancies.

At $x=1.25$, the anion vacancies have disappeared (see Fig. 6) and the cation vacancies may be ordered as shown in Fig. 10.[14] Here also the translational symmetry is compatible with lifting $2[V_C]$ orbitals from below to above the middle of the t_2^* bands, leaving the metal-metal bonding orbitals two-thirds filled. Quenching from 1300 °C gives disordered vacancies, but the concentration of trapped holes presumably remains $2[V_C]$. Nevertheless, a narrowing of the metal-metal bonding bands together with increased elastic and electrostatic interactions between the vacancies make the disordered crystal metastable relative to the ordered crystal at room temperature.

In the range $(0.6) < x < 1.25$, both cation and anion vacancies are present. Even if two electrons are trapped at each anion vacancy, the stability of these trapped electrons is less than that of O^{2-} $2p$ electrons. Since the number of oxygen vacancies decreases with x, the binding energy should increase with x, a conclusion that is compatible with the observed variation of lattice parameter with x, as may be seen from Fig. 6. Without this

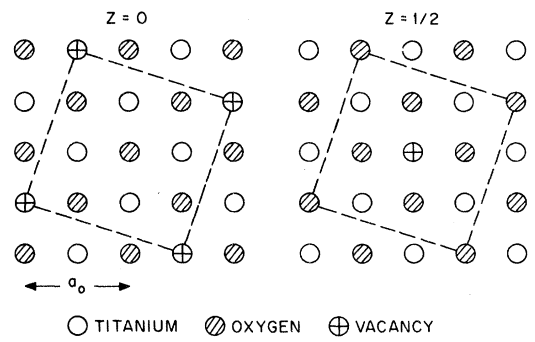

FIG. 10. The $z=0$ and $z=\frac{1}{2}$ planes of vacancy-ordered $TiO_{1.25}$. After Ref. 14.

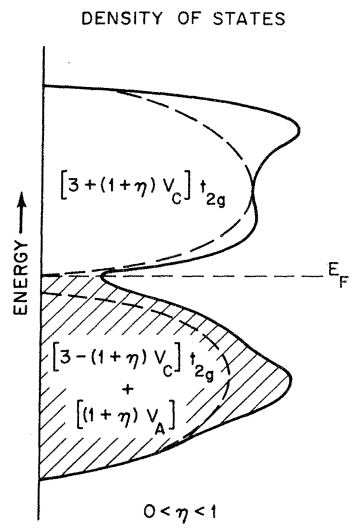

FIG. 11. Proposed density of states near E_F for stoichiometric VO, where $V_C = V_A$.

change in binding energy, the lattice parameter would increase with x, or with decreasing concentration of anion vacancies. In crystals containing disordered vacancies, the trap orbitals would have a wider range of energies, so that not every vacancy would trap two electrons and two holes. In this case, the Fermi energy would be raised somewhat with decreasing x. Nevertheless, the itinerant-electron t_2^* orbitals would remain less than half-filled. The fact that the Seebeck coefficient θ remains negative for all x (see Fig. 6) is consistent with a metallic expression[15]

$$\theta = \frac{\pi^2}{3}\,\frac{k^2 T}{e}\left(\frac{d\ln\sigma}{dE}\right)_{E=E_F}, \qquad (23)$$

since from Fig. 6 the conductivity σ increases with decreasing x and the electronic charge e is negative. This variation of σ with x is compatible with itinerant d electrons, the mobility $\mu = e\tau/m^*$ decreasing with τ as the number of cation vacancies, which act as primary scattering centers, increases.

C. VO_x

The situation in VO_x should be similar to that in TiO_x. However, there are four significant differences: (i) There is one more d electron per cation in VO_x than in TiO_x. (ii) The metal-metal separation increases with x from $R \approx 2.84$ to $R \approx 2.93$ Å, and my estimated critical separation for V^{2+} ions in oxides at room temperature and atmospheric pressure was $R_c \approx 2.92$ Å. Therefore, electron correlations due to a $U \neq 0$ are more probable in VO_x. (iii) The $3d$ orbitals are more stable relative to the $4s$ orbitals in VO_x, which means that $3d$-$4s$ hybridization is weaker. In addition, the effective nuclear charge seen by any $3d$ electron is larger in VO_x. Therefore the anion-vacancy trap orbitals are less stable relative to the middle of the t_2^* bands of Fig. 2(b), especially the second trap orbital because of a larger electrostatic energy U'. (iv) Only the compound $VO_{1.27}$ has been reported to order at low temperatures,[16] even though slow cooling and low-temperature annealing are possible in this system.

Figure 11 illustrates a qualitative density-of-states vs energy curve for stoichiometric VO. It is to be compared with Fig. 9(b) for disordered TiO. One trapped hole per cation vacancy and one trapped electron per anion vacancy are again assumed. Furthermore, the number of second-hole and second-electron trap states are also assumed to be reduced by the disorder and to be spread over a broader range of energies than in ordered TiO. Hole and electron trap states tend to annihilate each other if cation and anion vacancies occupy nearest-neighbor lattice sites. As in ideal VO, the three outer d electrons per V^{2+} ion in real VO just half-fill the itinerant-electron t_2^* bands, since the number of trapped holes and electrons are equal. Annihilation of hole and electron trap states occurs in pairs. Since a $U \neq 0$ is anticipated, a small energy gap is assumed to exist in the density of itinerant-electron states at E_F, in accordance with Fig. 3 for $b \approx b_g$. However, localized cation-vacancy trap states at the bottom of the upper band and localized anion-vacancy trap states at the top of the lower band would have energies overlapping this gap, since the vacancies are disordered. These localized states in wings at the edges of the bands are characteristic of amorphous compounds, where the electron potential varies from one atomic site to the next. Disordered vacancies create a variation in the potential at different cation-lattice sites, and the localized states in these wings may be similar to those occurring in amorphous materials, as has been pointed out to me by Mott.[17]

Figure 12 illustrates the density of states near the Fermi energy E_F for (a) $x < 1$ and (b) $x > 1$. In the region $x < 1$, the vacancy concentrations are $V_C < V_A$, and the second-hole trap levels at the cation vacancies tend to all be annihilated by nearest-neighbor anion vacancies. In the region $x > 1$, where $V_C > V_A$, the second-electron trap levels tend to be all annihilated. Nevertheless the Fermi energy E_F remains between the bonding and antibonding t_2^* bands so long as the second-trap-state energies do not overlap E_F. The semimetallic character of VO_x for $x < 1$ indicates that the second-electron trap states overlap E_F. It follows that $dE_F/dx < 0$ for $x < 1$. The semiconducting character of VO_x for $x > 1$, on the other hand, indicates that the second-hole trap states are essentially all above E_F, so that the Fermi energy remains pinned be-

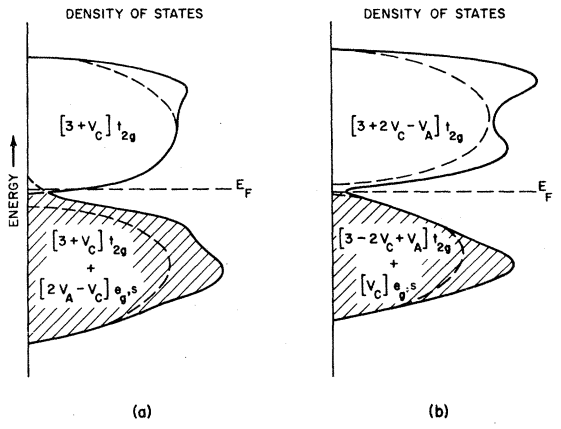

FIG. 12. Proposed density of states near E_F for the system VO_x: (a) $x<1$, where $V_C<V_A$ and (b) $x>1$, where $V_C>V_A$.

tween the bonding and antibonding t_2^* bands where $x>1$.

The remaining problem is to see whether these qualitative arguments are consistent with the measured properties of VO_x. From Fig. 6, the lattice parameters for the system VO_x, unlike those for TiO_x, increase with x. In this system the influence of ionic size outweighs the reduction in binding energy that occurs if anion vacancies are introduced. This change in the relative influence of ionic size is due in part to the greater relative stability of the vanadium $3d$ electrons; but it must also be due in part to the smaller size of the V^{2+} ion, which makes the lattice parameter more sensitive to oxygen-oxygen repulsive forces.

The transport properties of the system VO_x support the model of Figs. 11 and 12, in which a $U\neq 0$ is assumed to open a small energy gap in the itinerant-electron bands, the energy gap increasing with metal-metal separation R, and hence with x. For $x<1$, E_F lies above the energy gap, and the electrical conductivity is dominated by itinerant electrons in the upper itinerant-electron band. Therefore, the Seebeck coefficient is negative, and at smallest x its magnitude increases linearly with temperature as for a metal. However, because of the presence of localized trap states at the Fermi energy, the electron mobilities are low and VO_x exhibits the properties of a poor metal. For $x>1.0$, on the other hand, E_F drops below the bottom of the upper band, and the electrical conductivity is dominated at room temperature by higher-mobility itinerant holes in the lower t_2^* band, the localized defect states acting as acceptor states. Therefore, the room-temperature Seebeck coefficient is positive, although at low temperatures where conduction is dominated by hopping of electrons between trap states, it may become negative for $x\leq 1.15$. At larger x, where the second-electron trap states are completely annihilated, the Fermi energy drops to the top of the lower t_2^* band, and the Seebeck coefficient appears to be positive for all temperature and to increase linearly with temperature in the measured range $77<T<375$ °K. The asymptotic high-temperature activation energy for conduction, which is plotted in Fig. 6, increases linearly with x, and hence with the metal-metal separation R. This observation is consistent with an energy gap in the itinerant t_2^* band that increases with R, in accordance with an increasing $U\neq 0$ as $R\rightarrow R_c$.

A characteristic feature of the $\ln\rho$ vs $1/T$ plots for $x>1$ is the lack of a straight line, the effective activation energy decreasing with temperature.[9] Mott[17] has suggested that the low-temperature conductivity may be well described by

$$\sigma\propto e^{-b/T^{1/4}}, \tag{24}$$

which he[18] has shown to be characteristic of conduction by localized states in amorphous materials. Although $\ln\sigma=a-bT^{-n}$ shows $n\approx 1.56x+1.47$ for $0.99\leq x\leq 1.30$ ($n=-\frac{1}{4}$ only at $x=1.1$), nevertheless this provides striking support for the presence of localized states at E_F in the interval $1<x<1.2$, in accord with the prediction of Fig. 12(b).

This model depends upon some physical mechanism to split the t_2^* bands in two, such as a $b\lesssim b_g$ according to Fig. 3. Although a $U\neq 0$ is consistent with an $R\rightarrow R_c$ as $x\rightarrow 1.30$, nevertheless it makes requirements on the magnetic properties. A $U\neq 0$ should introduce an exchange enhancement into the magnetic susceptibility, thereby making it temperature-dependent. Furthermore, a $b_m\gtrsim b_g$ would require antiferromagnetic ordering at lowest temperatures.

Banus and Reed[8] have reported a temperature-dependent susceptibility. It can be expressed in the form

$$\chi=\chi_0+C/(T+\theta), \tag{25}$$

where the parameters χ_0, C, and θ are listed in Table I. Both the temperature-independent term χ_0 and the effective Curie constant C increase exponentially with x, which clearly indicates the presence of an exchange enhancement that increases

TABLE I. Composition dependence of the parameters χ_0, C, and θ of Eq. (25) for the systems VO_x [after M. D. Banus (private communication)]. For $x<1$, x_0 and C decrease monotonically with x, but $\theta\sim|1-x|$.

x	1.00	1.02	1.07	1.12	1.15	1.27	1.30	1.32
$\chi_0\times 10^3$ (emu/mole)	0.23	0.25	0.21	0.22	0.21	0.27	0.29	0.32
C(emu)	0.016	0.024	0.036	0.047	0.059	0.109	0.112	0.112
θ(°K)	1.4	2.4	3.2	4.3	4.3	6.8	7.5	7.9

with x. However, the low value of θ as well as the form of Eq. (25) are not what was anticipated from Fig. 5 and suggest that the moments contributing to the temperature-dependent term are relatively isolated from one another. This conclusion has been independently supported by ^{51}V NMR data.[19] Over the entire range of x, the Knight shift was $K < 0.4\%$ and proportional to χ_0. Such a small shift is compatible with E_F near a minimum in the density of states as well as with electron states that are primarily d-like. From the intensity of the temperature-independent NMR signal, Warren *et al.*[19] deduced that only a small proportion ($< 20\%$) of the vanadium sites carry localized moments. Perhaps even more significant is the lack of any antiferromagnetic ordering in disordered VO_x, even at large x. However, Kawano *et al.*[20] have reported definite evidence of antiferromagnetic ordering at low temperatures ($T_N \approx 4 - 7\,^\circ K$) in samples with largest x, T_N increasing with x. This low value of T_N is compatible with a small θ and suggests antiferromagnetic ordering between widely separated trap states. Whether this magnetic ordering is due to an ordering of the cation vacancies in these samples is not known. Stenstrom and Westman[16] have shown that vacancy ordering can be obtained in samples having $x \approx 1.27$.

These data lead to the conclusion that the localized moments contributing to the Curie constant C and the NMR line broadening are at cation-vacancy trap sites; presumably they represent occupied states in a cation-defect band that overlaps E_F. However, if this is true, then there is little magnetic evidence of a $U \neq 0$ associated with the itinerant-electron states. Thus any splitting of the t_2^* bands to produce an energy gap at or near E_F, which is so strongly suggested by the transport data, may not be due to a $U \neq 0$ as originally anticipated, but rather to the large concentration of cation vacancies, which increases with x as well as R. With more than 16% vacancies in an atomic array, the best basis orbitals for forming the t_2^* bands may not be localized crystal-field orbitals, but molecular orbitals associated with metal-metal pairs. As in amorphous germanium, covalent bonding between nearest-neighbor atoms may split the bonding orbitals from the antibonding orbitals.

Finally, it is interesting to note that localized spins are apparently not associated with partially filled anion-vacancy states. It was pointed out above that the anion-vacancy states contain considerable $4s$ character, so that anion-vacancy defect bands would be broader than cation-vacancy defect bands.

ACKNOWLEDGMENTS

I would like to thank N. F. Mott for a most stimulating correspondence on this problem and for permission to quote his suggestion of the analogy with amorphous materials.

---

†Work was sponsored by the Department of the Air Force.

[1]T. E. Norwood and J. L. Fry, Phys. Rev. B2, 472 (1970); T. M. Wilson, Intern. J. Quantum Chem. IIIS, 757 (1970).

[2]N. F. Mott, Proc. Phys. Soc. (London) A62, 416 (1949).

[3]J. B. Goodenough, J. M. Longo, and J. A. Kafalas, Mater. Res. Bull. 3, 471 (1968).

[4]J. Hubbard, Proc. Roy. Soc. (London) A276, 238 (1963); A277, 237 (1964); A281, 401 (1964); A285, 542 (1965); A296, 82 (1966); A296, 100 (1966).

[5]W. E. Evenson, J. R. Schrieffer, and S. Q. Wang, J. Appl. Phys. 41, 1199 (1970).

[6]F. R. de Boer, C. J. Schinkel, J. Biesterbos, and S. Proost, J. Appl. Phys. 40, 1049 (1969).

[7]W. M. Lomer, Proc. Phys. Soc. (London) 80, 489 (1962).

[8]M. D. Banus and T. B. Reed, *The Chemistry of Extended Defects*, edited by L. Eyring and M. O'Keefe (North-Holland, Amsterdam, 1970), p. 488.

[9]M. D. Banus, T. B. Reed, and A. J. Strauss, following paper, Phys. Rev. B5, 2775 (1972).

[10]M. D. Banus, Mater. Res. Bull. 3, 723 (1968).

[11]D. Watanabe, J. R. Castles, A. Jostsons, and A. S. Malin, Acta Cryst. 23, 307 (1967).

[12]J. M. Longo, P. M. Raccah, and J. B. Goodenough, Mater. Res. Bull. 4, 191 (1969).

[13]J. B. Goodenough, Czech. J. Phys. B17, 304 (1967).

[14]D. Watanabe, O. Terasaki, A. Jostsons, and J. R. Castles, J. Phys. Soc. Japan 25, 292 (1968).

[15]N. F. Mott and H. Jones, *The Theory of the Properties of Metals and Alloys* (Oxford U. P., Oxford, England, 1936), p. 310.

[16]G. Stenstrom and S. Westman, Acta Chem. Scand. 22, 1712 (1968).

[17]N. F. Mott (private communication).

[18]N. F. Mott, J. Non-Cryst. Solids 1, 1 (1969).

[19]W. W. Warren, Jr., A. C. Gossard, and M. D. Banus, J. Appl. Phys. 41, 881 (1970); S. Takeuchi and K. Suzuki, J. Japan Inst. Metals (Sendai) 33, 409 (1969).

[20]S. Kawano, K. Kosuge, and S. Kachi, J. Phys. Soc. Japan 21, 2744 (1966).